

Regime-Conditional Stabilisation of LLM-Augmented Cooperative Multi-Agent Reinforcement Learning

Faid Keddouri^{a,*}, Sohaib Houhou^a, Aissa Boulmerka^a, Nadir Farhi^b

^aNational School of Artificial Intelligence (ENSIA), Sidi Abdellah Campus, Algiers, Algeria

^bCosys-Grettia, Univ Gustave Eiffel, F-77454 Marne-la-Vallee, France.

Abstract

Large Language Models (LLMs) offer a natural interface for translating human objectives into reward signals for cooperative multi-agent reinforcement learning (MARL), yet the training-time dynamics of this integration remain poorly understood. We show that dynamically updating LLM-generated reward weights during off-policy MARL violates the stationarity assumption of Potential-Based Reward Shaping (PBRS) and contaminates the experience replay buffer, whose stored transitions carry reward labels computed under stale shaping weights. We characterise the result as a *regime-dependent* failure whose severity depends on how competent the unshaped baseline already is. To control it we propose two stabilisation strategies: a Phase-Based Freeze Schedule that enforces strict stationarity within training phases, and Exponential Moving Average (EMA) smoothing that bounds per-episode weight drift. We evaluate across three cooperative environments and five random seeds with QMIX, complemented by an exploratory VDN extension, yielding a three-regime taxonomy. In the *augmentative* regime (Simple Spread), where the baseline is functional (74.4%), EMA significantly improves success to 86.7% (+12.3 pp, $p < 0.01$) while naive dynamic updates collapse it to 15.2%. In the *essential* regime (Level-Based Foraging), where the baseline is broken (0.1%), any shaping unlocks the task (95.9% under EMA). In the *supplementary* regime (SMAC 3m), where the baseline is near-saturated (98.8%), stabilised shaping preserves performance (99.9%) while unstabilised shaping adds variance without gain. These findings establish reward-signal stationarity as a necessary design constraint and indicate that regime placement is a practical predictor of whether dynamic LLM shaping helps or harms.

Keywords: Multi-agent reinforcement learning, Potential-based reward shaping, Language-conditioned RL, Non-stationarity, QMIX, Human-in-the-loop

1. Introduction

Cooperative multi-agent reinforcement learning (MARL) has produced strong team behaviour in complex coordination tasks through value-decomposition methods such as QMIX (Rashid et al., 2018) and policy-gradient methods such as MAPPO (Yu et al., 2022). A persistent practical obstacle, however, is adapting a learned team policy to *shifting human objectives* without exhaustive retraining. Reward shaping is the natural lever: a human expresses a preference, and that preference is injected as an auxiliary learning signal. Yet manual reward design is notoriously difficult — hand-crafted rewards are error-prone, task-specific, and inaccessible to non-expert operators — which has motivated a rapidly growing line of work that places a Large Language Model (LLM) at this interface. LLMs have been used as proxy reward functions scored directly from textual task descriptions (Kwon et al., 2023), as generators of reward code

*Corresponding author.

Email address: faid.keddouri@ensia.edu.dz (Faid Keddouri)

for robotic skill synthesis (Yu et al., 2023), and as iterative reward designers — Eureka (Ma et al., 2024), Text2Reward (Xie et al., 2024), and the multi-agent LAMARL (Zhu et al., 2025) translate natural-language instructions into executable reward signals. These systems operate predominantly in single-agent or on-policy settings and do not examine what happens when shaping weights are *updated mid-training* inside an off-policy learner with experience replay.

The dynamic setting is not a corner case: it is the natural deployment mode of a language interface to reward. The very appeal of expressing objectives in natural language is that they can be *revised* — an operator monitoring a team of agents will want to shift emphasis from speed to safety, or from individual progress to global coverage, as circumstances change, without restarting a training run that may span days. Existing frameworks sidestep this by treating reward generation as an offline step that concludes before learning begins (or between entire training runs, in Eureka’s evolutionary loop). The moment weight updates move *inside* the training run, however, they interact with the machinery of off-policy learning, and that interaction has not been characterised.

This omission is consequential. Value-decomposition methods are off-policy by construction: their sample efficiency rests on an experience replay buffer that reuses transitions collected thousands of episodes earlier. The buffer stores transitions whose reward labels were computed under the shaping weights in force at collection time. When an LLM revises those weights during training, stored rewards become inconsistent with the current objective: a transition collected early is later sampled with a reward that no longer reflects the prevailing reward function. Potential-Based Reward Shaping (PBRS) (Ng et al., 1999) guarantees that shaping of the form $F(s, s') = \gamma\Phi(s') - \Phi(s)$ preserves the optimal policy, but only while the potential Φ is *stationary*. An LLM that re-issues weights periodically makes Φ time-varying, breaking this guarantee precisely in the algorithmic setting — off-policy replay — where the resulting inconsistency is most damaging.

We study this failure systematically and find that its severity is not uniform but *regime-dependent*: it is governed by how competent the unshaped baseline policy already is. This paper makes three contributions.

- **(C1) A three-regime taxonomy** of cooperative environments — *essential*, *augmentative*, and *supplementary* — that predicts whether dynamic LLM reward shaping unlocks a task, risks catastrophic collapse, or is redundant but harmless once stabilised. With one exemplar environment per regime, we advance the taxonomy as an organising hypothesis supported by three case studies rather than as an established law.
- **(C2) Two stabilisation strategies** that restore stationarity to the shaped potential: a *Phase-Based Freeze Schedule* enforcing strict stationarity within training phases, and *Exponential Moving Average (EMA)* smoothing bounding per-episode weight drift, with the smoothing factor selected by ablation ($\alpha = 0.2$).
- **(C3) A multi-condition empirical validation** across three cooperative environments (Simple Spread, Level-Based Foraging, SMAC 3m) and five random seeds with QMIX, complemented by an exploratory VDN extension that probes whether the taxonomy is specific to QMIX’s monotonic mixer.

The remainder of the paper is organised as follows. Section 2 reviews related work; Section 3 introduces the formal background; Section 4 presents the language-to-reward pipeline, the non-stationarity analysis, and the two stabilisation strategies; Section 5 reports the multi-environment results and the regime taxonomy; Section 6 covers interpretability and human-in-the-loop evaluation; Section 7 discusses implications and future directions; and Section 8 concludes.

2. Related Work

Cooperative MARL and value decomposition. Centralised Training with Decentralised Execution (CTDE) within the Decentralised Partially Observable Markov Decision Process (DecPOMDP) framework (Oliehoek and Amato, 2016) underpins modern cooperative MARL. On the policy-gradient side, MADDPG (Lowe et al., 2017) introduced centralised critics with decentralised actors, and MAPPO (Yu et al., 2022) showed that carefully tuned on-policy learning is competitive across standard benchmarks. On the value-based side, VDN (Sunehag et al., 2018) decomposes the joint action-value additively, QMIX (Rashid et al., 2018) factors it through a monotonic mixing network, and later work relaxes the monotonicity restriction — QTRAN (Son et al., 2019) via transformed factorisation objectives and QPLEX (Wang et al., 2021) via a duplex dueling architecture. Progress in this family has been driven substantially by standardised benchmarks such as the StarCraft Multi-Agent Challenge (Samvelyan et al., 2019), from which our SMAC 3m task is drawn. *Gap:* these methods assume a fixed team reward and do not study the interaction between a dynamically shifting reward function and the off-policy transitions stored under earlier objectives.

Potential-Based Reward Shaping. Ng et al. (Ng et al., 1999) proved that shaping rewards of the form $F = \gamma\Phi(s') - \Phi(s)$ leave the optimal policy invariant, *provided the potential Φ is stationary*, i.e. held fixed throughout learning. Static potential-based shaping was later shown to be equivalent to initialising the Q -function with Φ (Wiewiora, 2003), and the framework was extended so that arbitrary reward functions can be expressed as potential-based advice (Harutyunyan et al., 2015). Devlin and Kudenko (Devlin and Kudenko, 2012) extended the invariance guarantee to time-varying potentials in *on-policy* cooperative settings, where fresh interactions remain consistent with the current potential. *Gap:* this guarantee does not transfer to off-policy algorithms with experience replay, where stored transitions carry reward labels from earlier potentials and the telescoping sum that underlies policy invariance no longer cancels.

LLMs as reward designers. An LLM was first used as a proxy reward function that scores agent behaviour directly against a textual task description (Kwon et al., 2023); subsequent work translates language into reward code for real-time robotic skill synthesis (Yu et al., 2023). Eureka (Ma et al., 2024) couples LLM reward generation with evolutionary search over full reward programs, and Text2Reward (Xie et al., 2024) generates dense reward code refined by human feedback, both for single-agent tasks; LAMARL (Zhu et al., 2025) extends LLM-aided reward design to cooperative MARL. All of these systems revise rewards *between* training runs or before training begins, and they measure success by the semantic quality of the generated reward. *Gap:* none of these frameworks characterise the replay-buffer contamination that arises when LLM-produced reward weights shift mid-training in an off-policy learner, nor do they constrain LLM outputs to a stationarity-preserving potential.

Non-stationarity in multi-agent learning. Standard MARL non-stationarity arises from concurrently evolving policies: each agent’s environment shifts as its teammates learn (Hernandez-Leal et al., 2017). Experience replay can be stabilised against this policy-version drift by conditioning on a training-iteration fingerprint (Foerster et al., 2017) or by importance-weighting stale transitions. A separate line, Reinforcement Learning from Human Feedback (RLHF), learns reward models from human preference comparisons (Christiano et al., 2017) and now underpins the alignment of large language models themselves (Ouyang et al., 2022); there the reward model also evolves, but training is typically on-policy and the reward is inferred implicitly rather than issued as explicit weights. *Gap:* these approaches address *policy-version* non-stationarity or implicit reward inference; the failure studied here is *reward-label* non-stationarity injected by explicit external LLM weight updates, orthogonal to policy-version awareness.

Table 1: Table of notations.

Symbol	Meaning
G	Dec-POMDP tuple $\langle \mathcal{I}, \mathcal{S}, \mathcal{A}, P, R, \Omega, O, \gamma \rangle$
\mathcal{I}, n	set of agents and their number
\mathcal{S}, \mathcal{A}	state space and joint action space $A_1 \times \dots \times A_n$
P, R	transition function and shared team reward
Ω, O	observation space and observation function
γ	discount factor
$o_t^{(i)}, u_t^{(i)}$	observation and action of agent i at step t
τ_i, π_i	action-observation history and policy of agent i
Q_i, Q_{tot}	per-agent utility and joint action-value
Φ, F	shaping potential and PBRS reward $\gamma\Phi(s') - \Phi(s)$
$r_{\text{base}}, r_{\text{shaped}}$	unshaped team reward $R(s, \mathbf{u})$ and shaped reward $r_{\text{base}} + F$
I	natural-language operator instruction
$\phi(s), m$	feature-function vector $(\phi_1, \dots, \phi_m)^\top$ and its dimension ($m = 5$)
$\mathbf{w}, \mathbf{w}_{\text{LLM}}$	shaping weight vector in force and raw LLM output
α	EMA smoothing factor
$K, P_k, \mathbf{w}^{(k)}$	number of phases, k -th phase, and its frozen weights
T	training horizon in episodes
η, ε	learning rate and exploration rate
σ	cross-seed standard deviation

3. Background

Table 1 collects the notation used throughout the paper; each symbol is also defined in the text at its first occurrence.

Dec-POMDP. A cooperative multi-agent task is modelled as a Decentralised Partially Observable Markov Decision Process (Oliehoek and Amato, 2016) $G = \langle \mathcal{I}, \mathcal{S}, \mathcal{A}, P, R, \Omega, O, \gamma \rangle$, where \mathcal{I} is the set of n agents, \mathcal{S} the state space, $\mathcal{A} = A_1 \times \dots \times A_n$ the joint action space, P the transition function, $R : \mathcal{S} \times \mathcal{A} \rightarrow \mathbb{R}$ the shared team reward, Ω the observation space with observation function O , and $\gamma \in [0, 1)$ the discount factor. Agents share a common reward but each observes only part of the environment; agent i conditions its policy $\pi_i(u_i | \tau_i)$ on its local action-observation history τ_i . The team maximises the expected discounted return $J(\pi) = \mathbb{E}[\sum_{t=0}^{\infty} \gamma^t r_t]$.

Value decomposition. QMIX (Rashid et al., 2018) learns per-agent utilities $Q_i(\tau_i, u_i)$ and combines them through a monotonic mixing network into a joint action-value Q_{tot} , enforcing the Individual-Global-Max condition via the constraint $\partial Q_{\text{tot}} / \partial Q_i \geq 0$ so that decentralised greedy action selection is jointly optimal. VDN (Sunehag et al., 2018) is the special case $Q_{\text{tot}} = \sum_i Q_i$. Both are off-policy and trained from an experience replay buffer.

Potential-Based Reward Shaping. PBRS incorporates domain knowledge without altering the optimal policy. Ng et al. (Ng et al., 1999) proved that a shaping reward

$$F(s, s') = \gamma \Phi(s') - \Phi(s) \quad (1)$$

added to the environment reward leaves the optimal policy unchanged for any real-valued potential $\Phi : \mathcal{S} \rightarrow \mathbb{R}$, because its discounted contribution telescopes to a policy-independent constant determined by the initial state; they further showed that this potential-based form is

necessary for policy invariance under arbitrary dynamics. The guarantee, however, requires Φ to be *fixed* throughout learning. In MARL, PBRs likewise preserves Nash equilibria (Devlin and Kudenko, 2012), but again only under a stationary Φ . As Section 4 shows, LLM-produced dynamic weights make Φ time-varying and violate this assumption.

4. Methodology

We present the methodology in four parts: the language-to-reward pipeline that turns an instruction into a shaped reward (Section 4.1), the optimised QMIX backbone (Section 4.2), a mechanistic account of the non-stationarity that dynamic weight updates induce (Section 4.3), and the two stabilisation strategies that control it (Section 4.4).

4.1. Language-to-Reward Pipeline

The pipeline is built on a fixed vector of $m = 5$ bounded, interpretable feature functions $\phi(s) = (\phi_1(s), \dots, \phi_m(s))^\top$, each mapping the state to a scalar that captures one behavioural aspect of the task. Instantiated on Simple Spread, the five features are:

- ϕ_1 — *local proximity*: how close each agent is to its nearest landmark, rewarding individual progress towards coverage;
- ϕ_2 — *global coverage*: how well the team as a whole covers all landmarks, capturing the joint objective;
- ϕ_3 — *collision avoidance*: a penalty term that decreases the potential when agents crowd within collision distance of one another;
- ϕ_4 — *formation*: the spatial dispersion of the team, encouraging agents to spread out rather than cluster;
- ϕ_5 — *speed*: the agents’ movement magnitude, allowing an operator to trade urgency against safety.

The other environments instantiate the same five slots with domain analogues (e.g. proximity to food and joint-load readiness in LBF, target proximity and focus-fire concentration in SMAC 3m); the features are hand-designed once per environment and never change during training.

An LLM acts as a “Reward Architect”: given a high-level natural-language instruction I (e.g. “avoid collisions and focus on global coverage”), it outputs a structured weight vector with one component per feature of ϕ ,

$$\mathbf{w}_{\text{LLM}} = \text{LLM}(I) = \{w_{\text{local}}, w_{\text{global}}, w_{\text{collision}}, w_{\text{formation}}, w_{\text{speed}}\}, \quad (2)$$

whose $m = 5$ components form the weight vector $\mathbf{w} = (w_1, \dots, w_m)^\top$, so the named components of Equation (2) correspond one-to-one to ϕ_1, \dots, ϕ_5 above. Each weight is constrained to $w_j \in [0, 5]$: a bounded range caps the magnitude of the potential and hence of the shaping signal — together with the bounded features it keeps $|F|/|r_{\text{base}}| \approx 0.05$ (Section 4.3), so shaping can never dominate the base reward — while still spanning a factor-of-five contrast between de-emphasised and emphasised features. The coincidence between the upper bound 5 and the number of features $m = 5$ is incidental. As the reward architect we use Qwen 2.5 3B (Instruct) (Qwen Team, 2024) in 4-bit NF4 quantisation. The choice is driven by the nature of the task rather than by benchmark performance: translating a short instruction into a constrained JSON schema requires instruction-following, not open-ended reasoning, so a small open-weights model suffices; quantised, it occupies ≈ 1.91 GB of VRAM alongside training and answers in under 200 ms per query (Table 3), which makes even per-episode querying feasible. The LLM’s

role is strictly translational, decoupled from the RL gradient loop; robustness to the choice of reward architect is flagged as future work (Section 7). The weight vector parameterises a potential

$$\Phi(s; \mathbf{w}) = \sum_{j=1}^m w_j \phi_j(s) = \mathbf{w}^\top \boldsymbol{\phi}(s). \quad (3)$$

The complete information flow is

$$I \xrightarrow{\text{LLM}} \mathbf{w}_{\text{LLM}} \longrightarrow \Phi(\cdot; \mathbf{w}) \longrightarrow F(s, s') \longrightarrow r_{\text{shaped}} = r_{\text{base}} + F(s, s'), \quad (4)$$

where $r_{\text{base}} = R(s, \mathbf{u})$ denotes the unshaped team reward returned by the environment and F is the PBRS reward of Equation (1). Figure 1 illustrates the pipeline: the MARL training loop produces shaped rewards and updates policies through TD-error gradient steps, while the LLM module receives an instruction and returns a JSON weight vector. Crucially, no gradient signal flows back to the LLM — it remains frozen throughout training.

4.2. Optimised Recurrent QMIX Backbone

We build on QMIX with parameter-shared Gated Recurrent Unit (GRU) (Cho et al., 2014) agent networks. To resolve the perceptual aliasing that arises in symmetric environments — where agents receiving identical observations cannot differentiate their roles — we augment each agent’s input with a one-hot agent identity and its previous action:

$$\text{Input}_t^{(i)} = [o_t^{(i)}, \text{OneHot}(u_{t-1}^{(i)}), \text{OneHot}(i)]. \quad (5)$$

This enrichment raised the unshaped Simple Spread success rate from 55% to approximately 71% in early single-seed development (1,000 evaluation episodes), in line with QMIX benchmarks for this task (Papoudakis et al., 2021), though evaluation protocols differ (we use 200-episode greedy evaluation at each checkpoint), so the comparison is indicative rather than exact. The canonical five-seed baseline reported later (Figure 3) is $74.4 \pm 5.4\%$. All subsequent experiments use this backbone.

4.3. Non-Stationarity: A Mechanistic Account

Under standard PBRS the shaping reward of Equation (1) preserves optimal policies when Φ is stationary. When the LLM re-issues weights during training, the potential becomes time-dependent, $\Phi_t(s) = \mathbf{w}_t^\top \boldsymbol{\phi}(s)$ with $\mathbf{w}_t \neq \mathbf{w}_{t+1}$, and the per-step shaping reward is $F_t(s_t, s_{t+1}) = \gamma \Phi_t(s_{t+1}) - \Phi_t(s_t)$. The telescoping sum that underlies policy invariance then fails: in the discounted shaping return $\sum_t \gamma^t F_t$, the term $\gamma^{t+1} \Phi_t(s_{t+1})$ contributed at step t no longer cancels the term $-\gamma^{t+1} \Phi_{t+1}(s_{t+1})$ contributed at step $t+1$, leaving an uncanceled residual $\gamma^{t+1} [\Phi_t(s_{t+1}) - \Phi_{t+1}(s_{t+1})]$ at every interior state, so the shaped Markov decision process is no longer reward-equivalent to the original.

This violation compounds through four interacting mechanisms.

- **(i) PBRS guarantee violation.** With a stationary potential, the cumulative shaping reward telescopes to a policy-independent boundary term, so no policy is preferred over another on account of the shaping. Once Φ becomes time-varying, the uncanceled residuals derived above accumulate along trajectories, introducing a systematic bias that can steer the learned policy away from the optimum of the original task.
- **(ii) Replay-buffer contamination.** Off-policy learners store shaped rewards, not the quantities needed to recompute them. A transition stored at episode 1,000 carries a shaped reward computed with \mathbf{w}_{1000} ; when it is sampled later under \mathbf{w}_{5000} , the stored label no longer reflects the prevailing objective. With a 5,000-episode buffer (Table 2), every minibatch mixes reward semantics from up to 5,000 episodes of weight history, so gradients average over mutually inconsistent objectives.

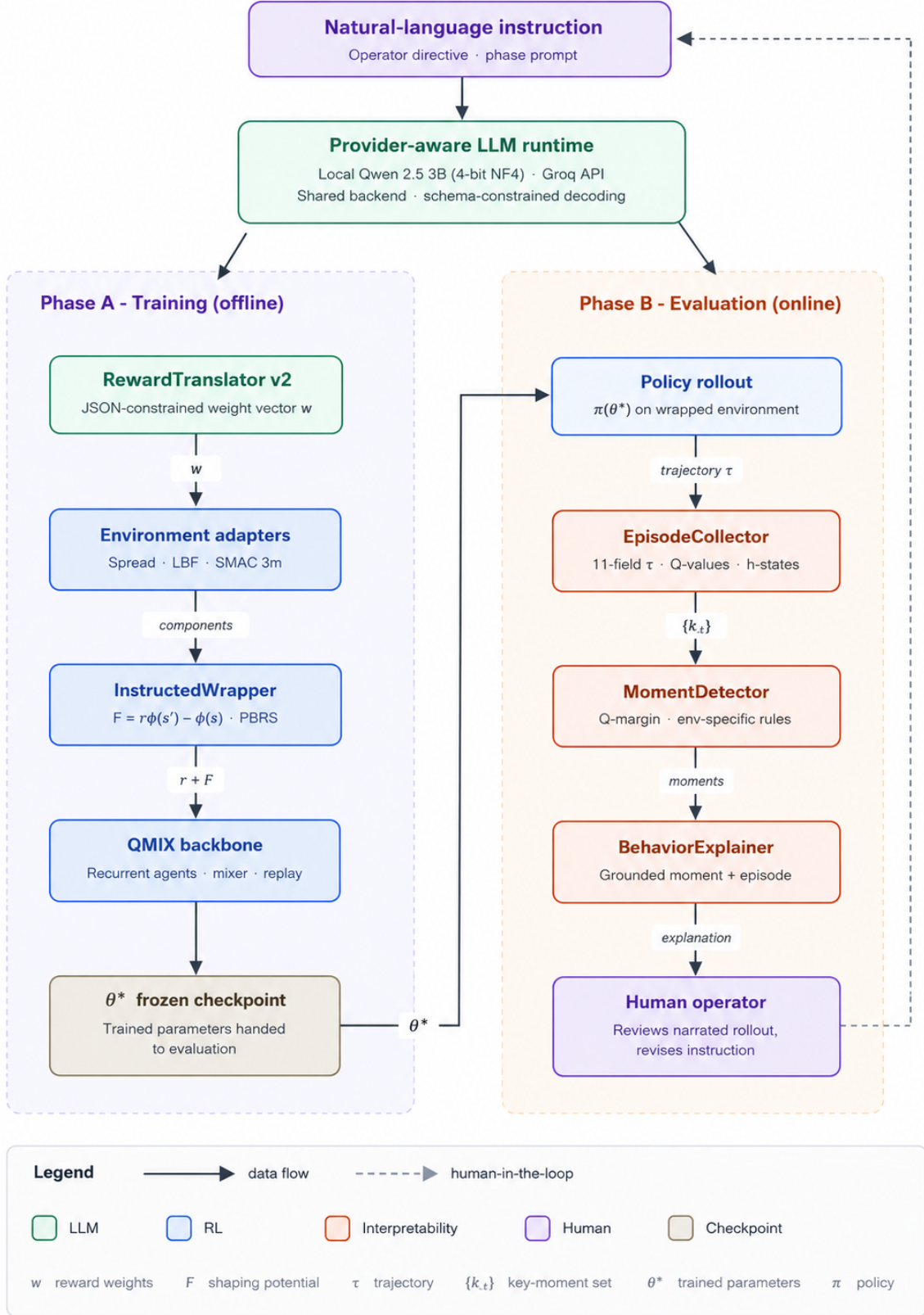


Figure 1: The provider-aware two-tier Language-to-Reward pipeline. *Phase A (training, offline)*: a natural-language instruction is translated by the LLM runtime into a JSON weight vector that parameterises the PBRs potential Φ , which shapes rewards for the QMIX backbone and yields a frozen checkpoint — no gradient flows back to the LLM. *Phase B (evaluation, online)*: the frozen policy is rolled out and an interpretability stack (EpisodeCollector → MomentDetector → BehaviorExplainer) produces natural-language audit narratives for a human operator.

- **(iii) Moving target.** Even setting the buffer aside, per-episode weight updates shift the reward function faster than the value function can adapt to it: agents chase a moving objective rather than converging on any single one, and improvements credited under one weight vector may be penalised under the next.
- **(iv) Value-function instability.** TD targets embed the shaping term F . When F changes between the moment a target is computed and the moment the corresponding gradient is applied — an interval stretched further by the hard target-network updates every 200 episodes — the regression targets themselves become noisy, inflating value-estimation variance on top of the bias from (i) and (ii).

A shaping-magnitude analysis confirms $|F|/|r_{\text{base}}| \approx 0.05$, ruling out reward domination: the failure arises from non-stationarity, not from the shaping signal overwhelming the base reward.

We are explicit about the scope of this account: it identifies the mechanisms at work and orders their interaction, but it does not quantify them. Deriving a formal bound on TD-target bias as a function of weight drift and replay-buffer age — the off-policy counterpart of the on-policy time-varying-potential guarantee of Devlin and Kudenko (Devlin and Kudenko, 2012) — is an open theoretical problem; the empirical study of Section 5 tests the account’s qualitative predictions instead.

4.4. Stabilisation Strategies

We propose two complementary strategies that restore stationarity during off-policy training, differing in the stationarity–adaptability trade-off.

Phase-Based Freeze Schedule. We partition the T -episode horizon into K contiguous phases P_1, P_2, \dots, P_K , where phase P_k covers episodes $t \in [(k-1)T/K, kT/K)$. At the boundary into phase P_k the LLM produces $\mathbf{w}^{(k)} = \text{LLM}(I_k)$ from the instruction I_k active at that point; within the phase, weights are frozen, $\mathbf{w}_t = \mathbf{w}^{(k)} \forall t \in P_k$. This guarantees a stationary Φ and exact PBRS invariance *within* each phase, at the cost of abrupt transitions between phases.

Exponential Moving Average (EMA) smoothing. EMA relaxes strict stationarity in favour of quasi-stationarity. Instead of applying \mathbf{w}_{LLM} directly, we blend each new target with the previous weights:

$$\mathbf{w}_t = \alpha \cdot \mathbf{w}_{\text{LLM}} + (1 - \alpha) \cdot \mathbf{w}_{t-1}, \quad (6)$$

with $\alpha \in (0, 1)$. Subtracting \mathbf{w}_{t-1} from Equation (6) gives $\mathbf{w}_t - \mathbf{w}_{t-1} = \alpha(\mathbf{w}_{\text{LLM}} - \mathbf{w}_{t-1})$, so the per-episode weight drift satisfies $\|\mathbf{w}_t - \mathbf{w}_{t-1}\| = \alpha\|\mathbf{w}_{\text{LLM}} - \mathbf{w}_{t-1}\|$, where $\|\cdot\|$ is the Euclidean norm. Since $\Phi_t(s) - \Phi_{t-1}(s) = (\mathbf{w}_t - \mathbf{w}_{t-1})^\top \phi(s)$, the Cauchy–Schwarz inequality bounds the induced potential drift, measured in the sup-norm $\|\Phi_t - \Phi_{t-1}\|_\infty = \max_s |\Phi_t(s) - \Phi_{t-1}(s)|$:

$$\|\Phi_t - \Phi_{t-1}\|_\infty \leq \alpha \|\mathbf{w}_{\text{LLM}} - \mathbf{w}_{t-1}\| \cdot \max_s \|\phi(s)\|, \quad (7)$$

which approaches zero as $\alpha \rightarrow 0$. Equation (7) controls the drift of the potential itself, not the downstream value-function bias; it should be read as a design principle — bounded drift — rather than a performance guarantee. We fix $\alpha = 0.2$ for all multi-seed experiments; Section 5.2 justifies this choice.

5. Experiments and Results

5.1. Experimental Setup

We evaluate on three cooperative environments spanning a wide range of baseline competence: Simple Spread (MPE), Level-Based Foraging (LBF), and SMAC 3m. Each method is

Table 2: Canonical QMIX configuration (shared across all conditions).

Hyperparameter	Value
Agent controller	FC \rightarrow GRU \rightarrow FC
GRU hidden dim	64
Mixer embedding dim	32
Optimiser	Adam
Learning rate	5×10^{-4}
Discount factor γ	0.99
Gradient clip	10.0
Batch size	32 episodes
Replay buffer	5,000 episodes
Target update	Hard, every 200 episodes
Exploration ϵ	1.0 \rightarrow 0.05 over 20k ep.
Training budget	100,000 episodes
Eval protocol	Greedy, 200 ep. / checkpoint

trained for 100,000 episodes across five random seeds $\{42, 101, 123, 456, 999\}$, and we report the mean \pm standard deviation. Evaluation uses a deterministic greedy policy ($\epsilon = 0$) over 200 episodes at each checkpoint. The reported metric is binary success rate for Simple Spread (all N landmarks covered) and LBF (≥ 1 food collected through valid joint loads), and win rate for SMAC 3m. Because MARL training exhibits seed variance, numbers should be compared *within* an environment, not across environments. We compare four conditions: Baseline (no shaping), Dynamic LLM (per-episode weight updates), and the two stabilised variants (Freeze-Schedule and EMA $\alpha = 0.2$). All four share the backbone and training budget of Table 2; the LLM configuration is given in Table 3 and the three environments in Table 4.

The Dynamic LLM condition. In the Dynamic LLM condition the reward architect is re-queried at every episode boundary, so the weight vector in force can change from one episode to the next. Two sources of variation are therefore present: scheduled revisions of the operator instruction over the course of training, and per-query sampling stochasticity of the LLM (temperature 0.1) under the instruction active at that point. Per-episode re-queried is deliberately the most aggressive schedule: no existing framework updates this frequently (Eureka revises rewards between training runs, LAMARL at coarser granularity), and we do not present it as a reproduction of any deployed system. It is instead the *limiting case* of the setting that motivates this work — real-time human-in-the-loop steering, in which an operator may revise the objective at any moment — and thus an upper bound on the update frequencies such a system could exhibit. The mechanistic account of Section 4.3 predicts that intermediate update frequencies (e.g., every few thousand episodes, without smoothing) interpolate between the Dynamic and Freeze-Schedule endpoints, and that collapse severity scales with replay-buffer age; testing these two causal predictions is left to future work (Section 7).

5.2. Selecting the Smoothing Factor

The value $\alpha = 0.2$ is not arbitrary. Before the multi-seed campaign, a diagnostic single-seed sweep on Simple Spread (same 100k-episode budget) evaluated $\alpha \in \{0.01, 0.05, 0.1, 0.2, 0.3, 0.5\}$ on four indicators: best success, final success, best return, and a composite ranking score used only for within-sweep model selection (Table 5). The landscape is *non-monotonic* (Figure 2): very small smoothing ($\alpha = 0.01$) under-adapts and is still improving at the horizon, while intermediate values ($\alpha = 0.1, 0.3$) exhibit severe late-stage regression despite respectable peaks. Only $\alpha = 0.2$ is jointly best on all four indicators, with a mere 2pp peak-to-final gap, so it is

Table 3: Canonical LLM (Reward Architect) configuration.

Parameter	Value
Model	Qwen 2.5 3B (Instruct)
Quantisation	4-bit NF4, fp16 compute
VRAM footprint	≈ 1.91 GB
Translation latency	≈ 200 ms / query
Translation temperature	0.1
Weight range	$w_j \in [0, 5]$
Output	JSON-only weight vector

Table 4: The three evaluated environments span the full range of baseline competence.

Property	Simple Spread	LBF 8×8-3p-2f	SMAC 3m
Backend	PettingZoo MPE	1bforaging v3	SMAClite
Agents	3	3	3 (Marines)
Observation	18-dim local	15-dim local	30-dim local
Actions	Discrete(5)	Discrete(6)	Discrete(9)
Horizon	25 steps	50 steps	~ 30 steps
Reward	Dense, per-step	Sparse on food load	Sparse: damage + win
Cooperation	Implicit (collisions)	Explicit (level-sum)	Implicit (focus-fire)
Regime	Augmentative	Essential	Supplementary
SR/WR _{base}	74.4%	$\approx 0\%$	98.8%

Table 5: Diagnostic EMA α ablation on Simple Spread (single seed, 100k episodes). Best row in bold.

α	Best success rate	Final success rate	Best return	Composite score
0.01	76.5%	76.0%	-30.86	0.671
0.05	82.0%	75.0%	-32.51	0.480
0.10	63.5%	42.0%	-32.79	0.150
0.20	88.0%	86.0%	-29.88	0.922
0.30	85.5%	57.5%	-31.45	0.592
0.50	85.0%	85.0%	-31.81	0.721

fixed for the canonical QMIX experiments and the exploratory VDN checks. The sharp contrast between neighbouring values — $\alpha = 0.1$ ends at 42.0% while $\alpha = 0.2$ ends at 86.0% — points to a sensitivity that a single seed cannot characterise, so a full multi-seed, cross-environment α -sweep remains future work; this diagnostic justifies the fixed value without claiming global optimality.

5.3. Overview of the Main Results

Figure 3 summarises the five-seed comparison across all three environments and all four conditions; the exact numerical values are collected in Table A.8 of Appendix A. Three patterns are visible at a glance and are unpacked in the subsections that follow: on Simple Spread the two stabilised methods beat the baseline while Dynamic LLM collapses; on LBF every shaping variant unlocks an otherwise broken task; and on SMAC 3m all methods sit near the ceiling, with Dynamic LLM alone showing inflated variance.

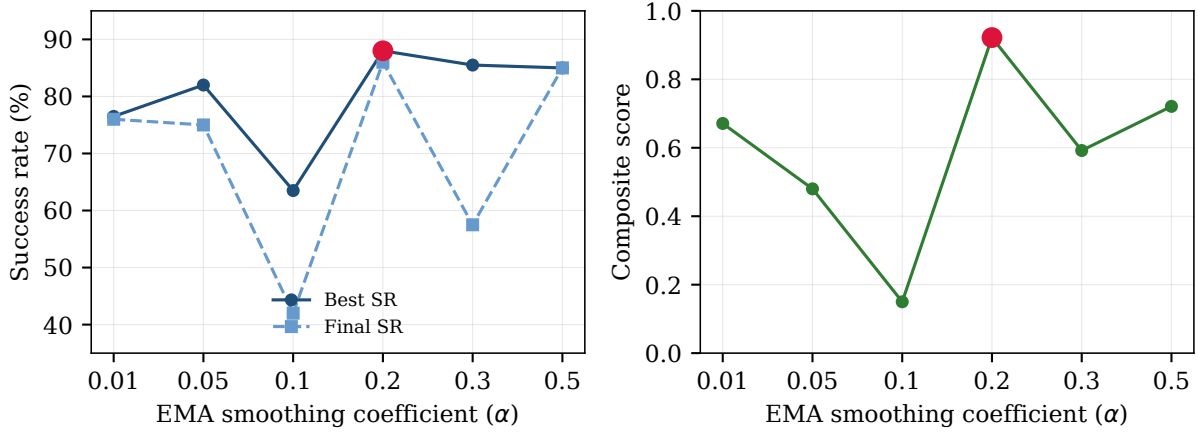


Figure 2: Diagnostic EMA α -ablation landscape on Simple Spread. *Left*: best and final success rates. *Right*: the composite ranking statistic used only for within-sweep model selection. The landscape is non-monotonic; $\alpha = 0.2$ (red marker) is jointly best on peak success, final success, return, and composite score.

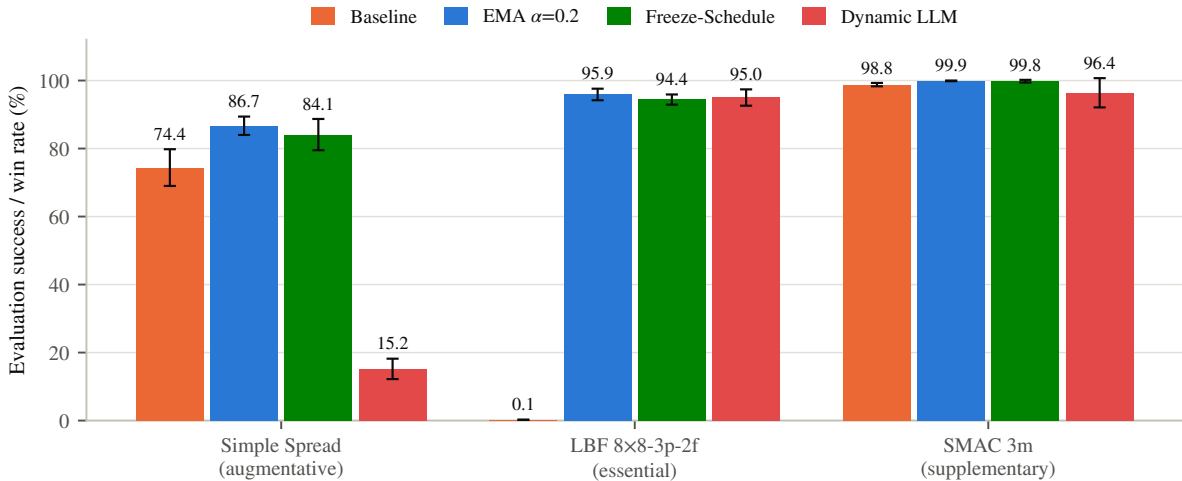


Figure 3: Main results: evaluation success rate (Simple Spread, LBF) and win rate (SMAC 3m) for all four conditions, five-seed mean with $\pm 1\sigma$ error bars (QMIX, $n = 5$ seeds). Exact values in Table A.8, Appendix Appendix A.

5.4. Simple Spread: the Augmentative Regime

Simple Spread requires $N = 3$ agents to each cover a distinct landmark while avoiding collisions. The unshaped baseline is already *functional* (74.4%), making this an augmentative regime in which shaping supplements an existing learning signal. The left group of Figure 3 reports the five-seed comparison and Figure 4 the training curves.

Both stabilised methods significantly outperform the baseline: EMA reaches 86.7 ± 2.7 (+12.3 pp, $p < 0.01$, Welch t -test) and Freeze-Schedule 84.1 ± 4.6 (+9.7 pp, $p < 0.05$). Notably, both exhibit *lower* cross-seed variance than the baseline itself ($\sigma = 2.7$ for EMA, 4.6 for Freeze, versus 5.4 for baseline), indicating that stationarity control also acts as a training regulariser. In sharp contrast, Dynamic LLM collapses to 15.2 ± 3.0 , a fall of 59.2 pp below baseline ($p < 0.001$). This is the defining hazard of the augmentative regime: because shaping only supplements an already-competent policy, the non-stationarity noise outweighs the shaping benefit. The pairwise Welch t -tests, visualised in Figure 5 (full statistics in Table A.9, Appendix Appendix A), confirm both stabilised gains are significant while the two stabilisers are statistically indistinguishable from each other.

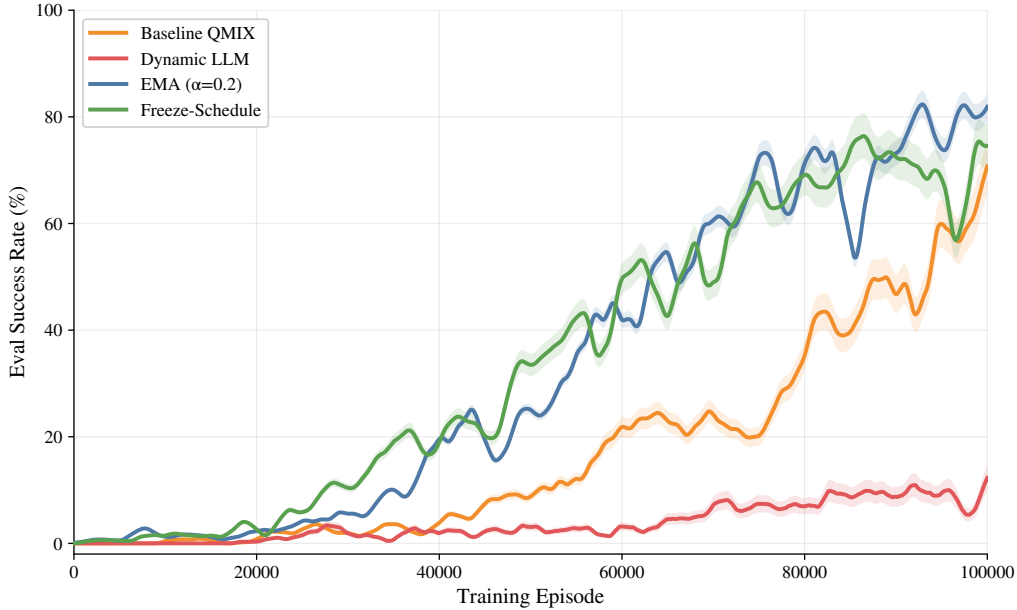


Figure 4: Simple Spread training curves, five seeds. Shaded bands denote $\pm 1\sigma$. Dynamic LLM (per-episode updates) collapses, whereas EMA and Freeze-Schedule both exceed the unshaped baseline.

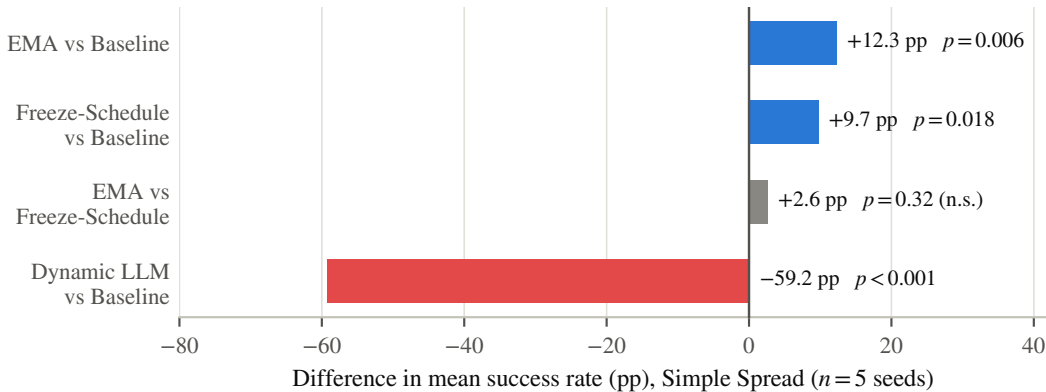


Figure 5: Pairwise Welch t -test outcomes on Simple Spread ($n = 5$ seeds per condition). Bars give the difference in mean success rate; blue marks significant gains, red the significant collapse, and grey a non-significant difference. Full test statistics in Table A.9, Appendix Appendix A.

5.5. Level-Based Foraging: the Essential Regime

Level-Based Foraging (8×8 -3p-2f) places three agents on a grid where collecting food requires *simultaneous* loading by enough agents that their combined levels exceed the food level. The cooperative behaviour is hidden behind a sparse mechanic that the unshaped policy almost never discovers within the training budget, making this an *essential* regime in which shaping provides the only viable learning signal. The centre group of Figure 3 and Figure 6 report the results.

The unshaped baseline is operationally broken, succeeding on only $0.1 \pm 0.2\%$ of episodes: without shaping, the level-sum coordination requirement is intractable within 100k episodes. All three shaping variants raise success above 94%, a gain of +95.8 pp under EMA. The defining feature of the essential regime is that *even Dynamic LLM works* ($95.0 \pm 2.4\%$): when the shaping signal is the sole route to any reward, its benefit dwarfs the non-stationarity noise that proved catastrophic on Simple Spread. EMA again attains the highest mean and the lowest cross-seed variance among the shaping methods.

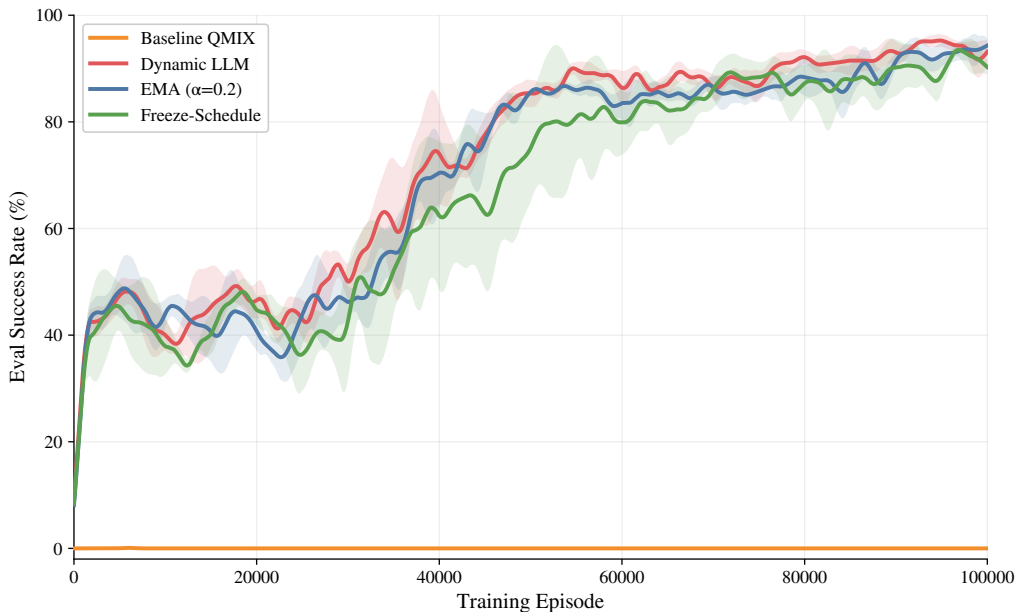


Figure 6: LBF 8×8 -3p-2f training curves, five seeds. The unshaped baseline never discovers joint-load success; all three shaping variants unlock the task.

A caveat on attribution is in order. The essential-regime gain demonstrates the power of PBRS with informative features on a sparse-reward task — a result in the spirit of (Ng et al., 1999) — rather than anything specific to the LLM: a hand-set static weight vector over the same features $\phi(s)$ would plausibly unlock the task as well. The LLM’s contribution here is the natural-language interface that produces and revises those weights without manual tuning; a no-LLM static-weight control that isolates this contribution is an experiment we have not run and flag as future work.

5.6. SMAC 3m: the Supplementary Regime

SMAC 3m is a 3-versus-3 StarCraft II micromanagement task in which three allied Marines must defeat three enemy Marines through focused fire and positioning. We use the SMAClite backend, a lightweight reimplement of SMAC; absolute win rates are therefore not directly comparable to published results on the original benchmark, and comparisons should once more be made within the environment. Baseline QMIX is already near-saturated, so shaping cannot meaningfully raise the mean; the regime is *supplementary*, and the relevant test is whether stabilisation *avoids harming* an already-strong policy. The right group of Figure 3 and Figure 7 report the results.

With a baseline of $98.8 \pm 0.5\%$, the EMA and Freeze gains (+1.1 pp and +1.0 pp) are not statistically significant — there is simply no headroom. The informative signal is in the tail: Dynamic LLM drops to $96.4 \pm 4.3\%$, adding substantial variance without any mean gain, while EMA and Freeze hold at 99.9% and 99.8% with negligible spread. In the supplementary regime, stabilised shaping passes the do-no-harm test that unstabilised dynamic updates fail.

5.7. Per-Seed Breakdown

Figure 8 plots the individual seed outcomes underlying the aggregate means above (numerical values in Table A.10, Appendix Appendix A). The Dynamic LLM collapse on Simple Spread is consistent across all five seeds (range 11.7–18.0%), ruling out a seed-specific artefact, and the LBF baseline rounds to zero on every seed.

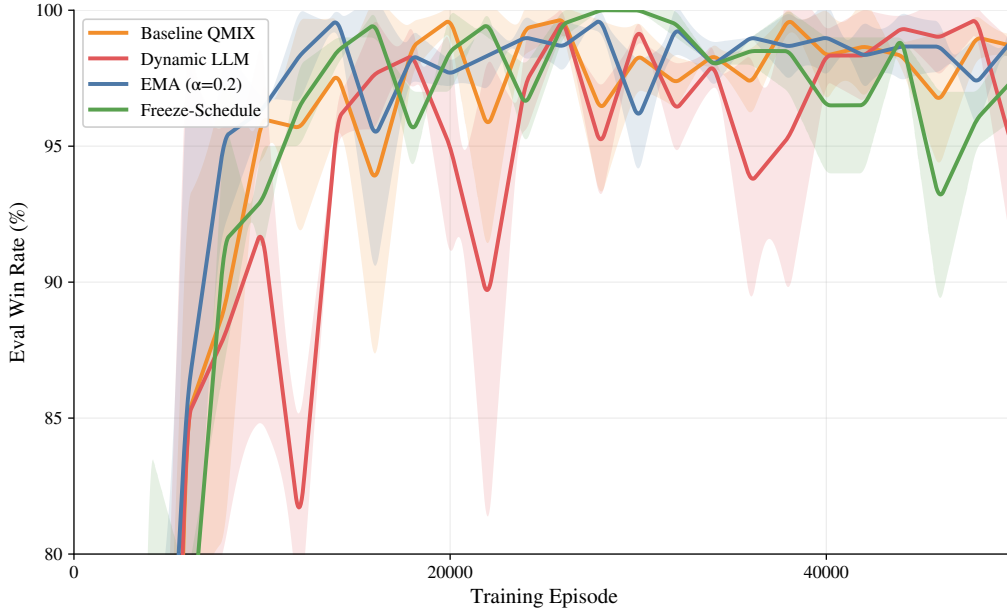


Figure 7: SMAC 3m training curves, shown with a zoomed 80–100% y -axis to expose post-convergence volatility; note that the truncated axis visually magnifies differences that are small in absolute terms. Win rates are near-ceiling; Dynamic LLM shows the largest fluctuations.

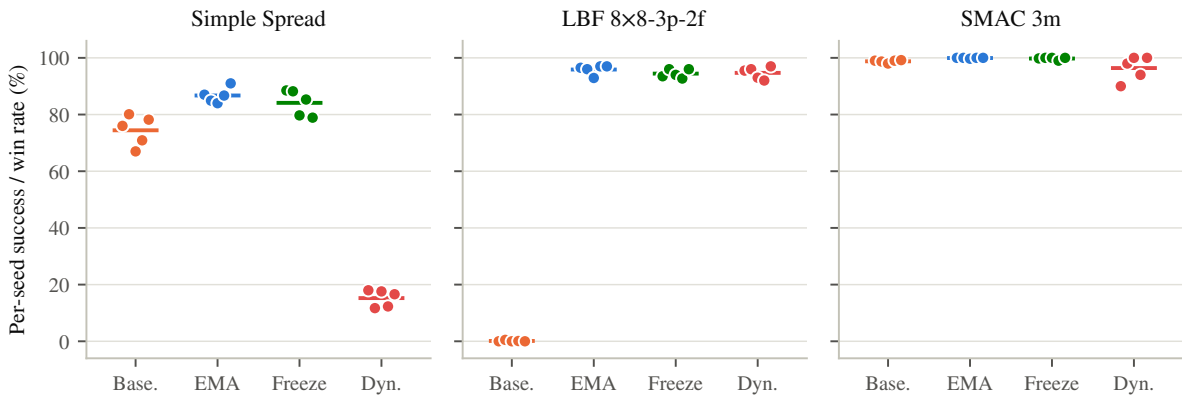


Figure 8: Per-seed evaluation outcomes for every environment and method (seeds 42/101/123/456/999); each dot is one seed and the horizontal bar the five-seed mean. Numerical values in Table A.10, Appendix Appendix A.

5.8. Exploratory VDN Results

A natural concern is that the regime taxonomy might be an artefact of QMIX’s monotonic mixing network rather than a property of the environments themselves. To probe this, we ran an exploratory extension in which the mixer is replaced by VDN’s simpler additive decomposition (Sunehag et al., 2018), while the backbone, training budget, shaping pipeline, and evaluation protocol all remain unchanged.

On two of the three environments, VDN reproduces the taxonomy. On Simple Spread, the ordering of conditions matches the QMIX study: EMA achieves the best mean ($81.6 \pm 4.3\%$), slightly above the unshaped baseline ($80.0 \pm 10.9\%$), while Dynamic LLM is both the weakest and the most variable condition ($75.2 \pm 10.8\%$). The collapse is milder than under QMIX, but the augmentative signature — stabilised shaping helps, unstabilised shaping hurts — is preserved. On SMAC 3m, VDN reproduces the supplementary ceiling: the baseline, EMA, and every completed Dynamic LLM seed reach a 100% win rate, leaving no headroom for shaping to add or remove.

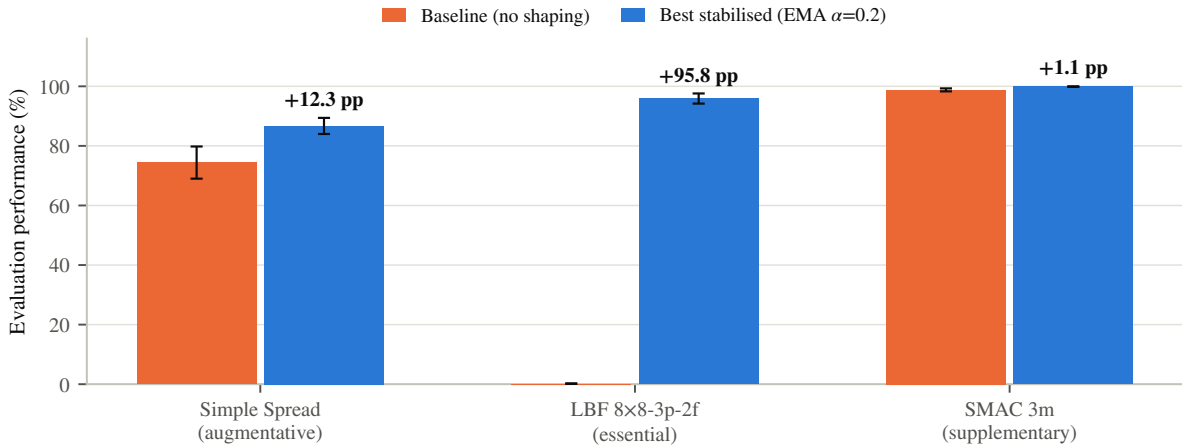


Figure 9: Cross-environment comparison underlying the regime taxonomy (QMIX, $n = 5$ seeds). Bars show mean $\pm 1\sigma$; the annotated deltas give the best stabilised gain over the unshaped baseline in each regime.

LBF is the exception: the shaped VDN runs did not complete reliably. The baseline reached $49.6 \pm 25.3\%$, only a single EMA seed produced a usable result (90.0%), and every Dynamic LLM seed failed. With so few completed runs, we draw no conclusion about the essential regime under VDN.

In summary, the VDN extension provides preliminary supporting evidence for the taxonomy on Simple Spread and SMAC 3m, but it is not an independent confirmation; every regime-level claim in this paper is anchored in the five-seed QMIX study.

5.9. The Regime Taxonomy

Synthesising the three environments yields a taxonomy organised by how competent the unshaped baseline already is (Figure 9; the placements are tabulated in Table A.11, Appendix Appendix A).

The three regimes are defined by baseline competence and predict the value — and danger — of dynamic LLM shaping. In the *essential* regime (LBF), the baseline is broken and any shaping unlocks the task, so even non-stationary updates help. In the *augmentative* regime (Simple Spread), the baseline is competent and shaping only supplements it; controlled shaping adds significant gains, but unstabilised dynamic updates collapse the policy. In the *supplementary* regime (SMAC 3m), the baseline is near-saturated and shaping is largely redundant; stabilised shaping is harmless, while unstabilised shaping injects variance. Regime placement, then, is a practical predictor of whether to apply dynamic LLM shaping and how aggressively to stabilise it.

An important qualification bounds this claim. With a single exemplar per regime, baseline competence is necessarily confounded with every other property that separates the three environments — reward density, horizon, observation dimensionality, and cooperation mechanic (Table 4). The taxonomy should therefore be read as an organising hypothesis that is consistent with, and motivated by, the three case studies, not as an established predictive law. Populating each regime with additional environments, or sweeping a single environment across regimes (for instance, varying LBF’s grid size and food levels moves its baseline from broken to functional), is the direct test we identify for future work.

6. Interpretability and Human-in-the-Loop Evaluation

Because the framework is meant to keep a human in the loop, reward control is paired with an interpretability subsystem: an *EpisodeCollector* records actions, Q-values, and task events;

Table 6: Cross-environment explainability profile ($n = 100$ episodes per environment).

Property	Simple Spread	LBF 8×8-3p-2f	SMAC 3m
Checkpoint	EMA, seed 42	EMA, seed 42	EMA, seed 456
Avg. episode length	25.0 / 25	48.7 / 50	19.0
Avg. key moments / ep.	8.66	5.28	12.00
Q-margin threshold τ_Q	0.30	0.50	1.00
Mean Q-margin	0.027	0.052	0.156
Top moment type	coverage	near_food	focus_fire
LLM narrative coverage	100%	100%	100%

Table 7: Post-instruction fine-tuning (5k episodes per instruction, frozen EMA s42 checkpoint). $\mathbf{w} = (w_\ell, w_g, w_c)$.

Instruction	\mathbf{w}	Pre SR	Post SR	Δ SR
Rush to landmark	(5, 0, 1)	80.0%	0.0%	−80.0
Avoid collisions	(0, 2, 5)	80.0%	0.5%	−79.5
Team coordination	(1, 5, 2)	80.0%	0.0%	−80.0

a *MomentDetector* flags decision-critical moments via per-environment Q-margin thresholds; and a *BehaviorExplainer* renders these into natural-language audit narratives. Applied to the best checkpoint of each environment over 100 evaluation episodes, the same three-component pipeline produces coherent narratives across all three regimes (Table 6). The mean Q-margin grows by an order of magnitude across environments ($0.027 \rightarrow 0.052 \rightarrow 0.156$), motivating per-environment threshold calibration; every episode received an LLM-generated narrative without fallback, at ≈ 1.91 GB GPU memory and ≈ 5 minutes per 100 episodes. Pairing each narrative with the structured `KeyMoment` ground truth makes the explanations auditable — a transparency prerequisite for deployment. The evaluations in this section re-load saved checkpoints and run independent 100–200-episode evaluations, so absolute rates differ by a few points from the best-checkpoint figures of Section 5.

6.1. Frozen-Policy Instruction Evaluation

On the frozen EMA seed-42 Spread checkpoint, ten operator instructions spanning speed, safety, and coordination intent were translated to weight vectors and each evaluated over 100 episodes. Success and collision rates were *identical* across all ten (SR = 0.85, CR = 0.22): with a frozen Q-network and an observation that excludes the instruction, action selection $\arg \max_a Q(\tau, u)$ cannot change. The shaped returns, however, differ per instruction (range -31.20 to -30.43 over an identical base return -31.74), confirming that the LLM produces semantically distinct \mathbf{w} . We report this honestly as instruction-aware *shaped-reward* evaluation, not online behavioural adaptation.

6.2. Post-Instruction Fine-Tuning

To test whether *unfreezing* the policy yields behavioural specialisation, we locked the weights to three contrasting instructions and continued training for 5k episodes, with learning rate $\eta = 10^{-4}$ and exploration rate ε annealed from 0.10 to 0.01. All three collapsed (Table 7). This honest negative result reinforces the central message: late-stage reward re-specification destabilises an off-policy learner exactly as mid-training non-stationarity does. It argues for evaluation-time interpretability and human override — rather than weight retraining — as the safe mode of human-in-the-loop control.

7. Discussion

A stability–quality paradox. The LLM-reward literature focuses on the *semantic quality* of generated rewards: Eureka searches evolutionary generations of reward programs for better-performing candidates, and Text2Reward refines reward code from human feedback, implicitly treating each revision as an improvement to be applied as soon as it is available. Our results show that in off-policy MARL the *stability* of the reward signal matters as much as its quality: even a well-designed reward causes catastrophic collapse if it is updated faster than the agent can adapt (Simple Spread, 74.4% \rightarrow 15.2%). The paradox is that a higher-quality revision, applied at the wrong cadence, is strictly worse than no revision at all. Reward-signal stationarity is therefore a first-class design constraint, not an implementation detail: any system that couples an LLM reward designer to an off-policy learner should specify an update budget — how often weights may change, and through what smoothing — with the same care it devotes to prompt design.

Stationarity–adaptability trade-off. The two stabilisers occupy different points on a continuum. The Freeze-Schedule enforces strict stationarity within each phase — exact PBRS invariance, at the price of discontinuities at phase boundaries — while EMA admits a small, bounded drift at every episode, spreading each weight revision over roughly $1/\alpha$ episodes. That EMA (quasi-stationarity) slightly outperforms the Freeze-Schedule (strict stationarity) on Simple Spread suggests that moderate, controlled drift can act as an implicit curriculum rather than pure noise: the potential is always moving gently towards the operator’s intent, and the learner tracks it. The advantage is small and environment-dependent, but it indicates that the design goal is bounded drift, not its complete elimination — and that the smoothing factor α is the natural knob with which to position a system on this continuum.

Lightweight LLMs as reward architects. Constraining the LLM to emit a structured JSON weight vector within a fixed PBRS potential reduces the task to translation, so a 3B model suffices at < 200 ms per query with negligible compute. This is a deliberate trade against expressiveness: code-generating approaches such as Eureka and Text2Reward let the LLM write arbitrary reward programs, which is strictly more powerful but harder to audit and can introduce unbounded or non-potential terms that void the PBRS guarantee by construction. The weight-vector interface keeps every degree of freedom semantically meaningful and bounded — each w_j answers “how much does the operator currently care about feature ϕ_j ?” — which the interpretability subsystem of Section 6 exploits directly. Practically, the small footprint (≈ 1.91 GB) means the reward architect runs on the same consumer GPU as training, with no external API dependency, which matters for on-premise and latency-sensitive deployments.

Future directions. The present study anchors the regime taxonomy in a single LLM, three environments, and small teams, which opens several natural extensions. First, sharpening the taxonomy’s evidential basis: populating each regime with at least two environments, or sweeping a single environment across regimes (varying LBF’s grid size and food levels moves its baseline from broken to functional at modest cost), would disentangle baseline competence from the other properties on which the three environments differ. Second, converting the mechanistic account of Section 4.3 from asserted to demonstrated: the account predicts that intermediate update frequencies without smoothing (e.g., every 1k–5k episodes) interpolate between the Dynamic and Freeze-Schedule endpoints, and that collapse severity scales with replay-buffer size — both are directly testable causal predictions. Third, isolating the LLM’s contribution with a static hand-set weight baseline over the same features, and testing robustness to the choice of reward architect beyond Qwen 2.5 3B. Fourth, establishing algorithm-agnosticism by completing the VDN sweeps on LBF and extending to policy-gradient methods such as MAPPO and richer decompositions such as QPLEX, together with a full multi-seed, cross-environment

sweep of the smoothing factor α (Section 5.2). Finally, the observation that bounded weight drift can act as an implicit curriculum invites deliberate curriculum design over the shaping weights, paired with real-time human-in-the-loop evaluation built on the interpretability stack of Section 6.

8. Conclusion

Per-episode LLM weight updates break the stationarity assumption of potential-based reward shaping and collapse task performance in the augmentative regime (74.4% \rightarrow 15.2% on Simple Spread). Two stabilisation strategies restore it: a Phase-Based Freeze Schedule and EMA smoothing ($\alpha = 0.2$), the latter reaching 86.7% on Simple Spread, 95.9% on Level-Based Foraging, and 99.9% on SMAC 3m. Across three environments and five seeds with QMIX — with exploratory VDN support — the results motivate a three-regime taxonomy (essential, augmentative, supplementary) that predicts when dynamic LLM shaping helps, when it is dangerous, and when it is merely redundant; with one environment per regime, we advance it as an organising hypothesis whose predictive scope remains to be established. The broader lesson is that reward-signal stationarity is a necessary design constraint for any system that combines LLM-guided reward shaping with off-policy experience replay. Future work will test the mechanism’s causal predictions (intermediate update frequencies and buffer-size ablations), add static-weight and multi-LLM controls, populate each regime with further environments, complete the VDN sweeps, extend to MAPPO and QPLEX, and develop real-time human-in-the-loop evaluation.

Acknowledgements

This work was carried out partially using the AI Datacenter of the National School of Artificial Intelligence, funded under grant number E049 24 0117 by the Algerian Ministry of Higher Education and Scientific Research.

Declarations

- **Funding.** This work was supported by the Algerian Ministry of Higher Education and Scientific Research under grant number E049 24 0117 (AI Datacenter, National School of Artificial Intelligence).
- **Competing interests.** The authors declare that they have no competing interests.
- **Ethics approval and consent to participate.** Not applicable.
- **Consent for publication.** Not applicable.
- **Data availability.** The training logs and experimental configurations supporting the findings of this paper will be released in a public repository upon acceptance; until then they are available from the authors upon reasonable request.
- **Materials availability.** Not applicable.
- **Code availability.** The full codebase will be released in a public repository upon acceptance; until then it is available from the authors upon reasonable request.
- **Author contribution.** F. Keddouri and S. Houhou designed and implemented the framework, ran the experiments, and drafted the manuscript. A. Boulmerka and N. Farhi supervised the work, advised on methodology and evaluation, and revised the manuscript. All authors read and approved the final manuscript.

References

- Kyunghyun Cho, Bart van Merriënboer, Caglar Gulcehre, Dzmitry Bahdanau, Fethi Bougares, Holger Schwenk, and Yoshua Bengio. Learning phrase representations using RNN encoder–decoder for statistical machine translation. In *Proceedings of the 2014 Conference on Empirical Methods in Natural Language Processing (EMNLP)*, pages 1724–1734, 2014.
- Paul F. Christiano, Jan Leike, Tom B. Brown, Miljan Martic, Shane Legg, and Dario Amodei. Deep reinforcement learning from human preferences. In *Advances in Neural Information Processing Systems (NeurIPS)*, volume 30, pages 4299–4307, 2017.
- Sam Devlin and Daniel Kudenko. Dynamic potential-based reward shaping. In *Proceedings of the 11th International Conference on Autonomous Agents and Multiagent Systems (AAMAS)*, pages 433–440, 2012.
- Jakob Foerster, Nantas Nardelli, Gregory Farquhar, Triantafyllos Afouras, Philip H. S. Torr, Pushmeet Kohli, and Shimon Whiteson. Stabilising experience replay for deep multi-agent reinforcement learning. In *Proceedings of the 34th International Conference on Machine Learning (ICML)*, pages 1146–1155, 2017.
- Anna Harutyunyan, Sam Devlin, Peter Vrancx, and Ann Nowé. Expressing arbitrary reward functions as potential-based advice. In *Proceedings of the 29th AAAI Conference on Artificial Intelligence*, pages 2652–2658, 2015.
- Pablo Hernandez-Leal, Michael Kaisers, Tim Baarslag, and Enrique Munoz de Cote. A survey of learning in multiagent environments: Dealing with non-stationarity. *arXiv preprint*, 2017. arXiv:1707.09183.
- Minae Kwon, Sang Michael Xie, Kalesha Bullard, and Dorsa Sadigh. Reward design with language models. In *Proceedings of the International Conference on Learning Representations (ICLR)*, 2023.
- Ryan Lowe, Yi Wu, Aviv Tamar, Jean Harb, Pieter Abbeel, and Igor Mordatch. Multi-agent actor-critic for mixed cooperative-competitive environments. In *Advances in Neural Information Processing Systems (NeurIPS)*, volume 30, pages 6379–6390, 2017.
- Yecheng Jason Ma, William Liang, Guanzhi Wang, De-An Huang, Osbert Bastani, Dinesh Jayaraman, Yuke Zhu, Linxi Fan, and Anima Anandkumar. Eureka: Human-level reward design via coding large language models. In *Proceedings of the International Conference on Learning Representations (ICLR)*, 2024.
- Andrew Y. Ng, Daishi Harada, and Stuart Russell. Policy invariance under reward transformations: Theory and application to reward shaping. In *Proceedings of the 16th International Conference on Machine Learning (ICML)*, pages 278–287, 1999.
- Frans A. Oliehoek and Christopher Amato. *A Concise Introduction to Decentralized POMDPs*. Springer, 2016.
- Long Ouyang, Jeffrey Wu, Xu Jiang, Diogo Almeida, Carroll Wainwright, Pamela Mishkin, Chong Zhang, Sandhini Agarwal, Katarina Slama, Alex Ray, et al. Training language models to follow instructions with human feedback. In *Advances in Neural Information Processing Systems (NeurIPS)*, volume 35, pages 27730–27744, 2022.

- Georgios Papoudakis, Filippos Christianos, Lukas Schäfer, and Stefano V. Albrecht. Benchmarking multi-agent deep reinforcement learning algorithms in cooperative tasks. In *Proceedings of the Neural Information Processing Systems Track on Datasets and Benchmarks (NeurIPS D&B)*, 2021.
- Qwen Team. Qwen2.5 technical report. Technical report, Alibaba Group, 2024. arXiv preprint arXiv:2412.15115.
- Tabish Rashid, Mikayel Samvelyan, Christian Schroeder de Witt, Gregory Farquhar, Jakob Foerster, and Shimon Whiteson. QMIX: Monotonic value function factorisation for deep multi-agent reinforcement learning. In *Proceedings of the 35th International Conference on Machine Learning (ICML)*, pages 4295–4304, 2018.
- Mikayel Samvelyan, Tabish Rashid, Christian Schroeder de Witt, Gregory Farquhar, Nantas Nardelli, Tim G. J. Rudner, Chia-Man Hung, Philip H. S. Torr, Jakob Foerster, and Shimon Whiteson. The StarCraft multi-agent challenge. In *Proceedings of the 18th International Conference on Autonomous Agents and Multiagent Systems (AAMAS), Extended Abstract*, pages 2186–2188, 2019.
- Kyunghwan Son, Daewoo Kim, Wan Ju Kang, David Hostallero, and Yung Yi. QTRAN: Learning to factorize with transformation for cooperative multi-agent reinforcement learning. In *Proceedings of the 36th International Conference on Machine Learning (ICML)*, pages 5887–5896, 2019.
- Peter Sunehag, Guy Lever, Audrunas Gruslys, Wojciech Marian Czarnecki, Vinicius Zambaldi, Max Jaderberg, Marc Lanctot, Nicolas Sonnerat, Joel Z. Leibo, Karl Tuyls, and Thore Graepel. Value-decomposition networks for cooperative multi-agent learning based on team reward. In *Proceedings of the 17th International Conference on Autonomous Agents and Multiagent Systems (AAMAS)*, pages 2085–2087, 2018.
- Jianhao Wang, Zhizhou Ren, Terry Liu, Yang Yu, and Chongjie Zhang. QPLEX: Duplex dueling multi-agent Q-learning. In *Proceedings of the International Conference on Learning Representations (ICLR)*, 2021.
- Eric Wiewiora. Potential-based shaping and Q-value initialization are equivalent. *Journal of Artificial Intelligence Research*, 19:205–208, 2003.
- Tianbao Xie, Siheng Zhao, Chen Henry Wu, Yitao Liu, Qian Luo, Victor Zhong, Yanchao Yang, and Tao Yu. Text2Reward: Reward shaping with language models for reinforcement learning. In *Proceedings of the International Conference on Learning Representations (ICLR)*, 2024.
- Chao Yu, Akash Velu, Eugene Vinitsky, Jiaxuan Gao, Yu Wang, Alexandre Bayen, and Yi Wu. The surprising effectiveness of PPO in cooperative multi-agent games. In *Advances in Neural Information Processing Systems (NeurIPS), Datasets and Benchmarks Track*, 2022.
- Wenhao Yu, Nimrod Gileadi, Chuyuan Fu, Sean Kirmani, Kuang-Huei Lee, Montserrat Gonzalez Arenas, Hao-Tien Lewis Chiang, Tom Erez, Leonard Hasenclever, Jan Humplik, Dorsa Sadigh, et al. Language to rewards for robotic skill synthesis. In *Proceedings of the 7th Conference on Robot Learning (CoRL)*, 2023.
- Guobin Zhu, Rui Wang, Sankai Liu, Fei Zhang, Zhen Han, and Shuai Sun. LAMARL: LLM-aided multi-agent reinforcement learning for cooperative policy generation. *arXiv preprint*, 2025. arXiv:2506.01538.

Appendix A. Numerical Result Tables

This appendix collects the numerical values underlying the result figures of Section 5. Table A.8 merges the per-environment five-seed comparisons visualised in Figure 3; Table A.9 gives the full Welch t -test statistics behind Figure 5; Table A.10 lists the per-seed outcomes plotted in Figure 8; and Table A.11 tabulates the regime placements of Figure 9.

Table A.8: Five-seed comparison across all three environments (QMIX, $n = 5$, seeds 42/101/123/456/999; mean \pm std). Eval success rate (%) for Simple Spread and LBF, win rate (%) for SMAC 3m. Best method per environment in bold.

Method	Simple Spread SR (%)	LBF 8 \times 8-3p-2f SR (%)	SMAC 3m WR (%)
Baseline QMIX (no shaping)	74.4 \pm 5.4	0.1 \pm 0.2	98.8 \pm 0.5
EMA $\alpha = 0.2$	86.7 \pm 2.7	95.9 \pm 1.7	99.9 \pm 0.1
Freeze-Schedule	84.1 \pm 4.6	94.4 \pm 1.5	99.8 \pm 0.4
Dynamic LLM (per-episode)	15.2 \pm 3.0	95.0 \pm 2.4	96.4 \pm 4.3

Table A.9: Pairwise Welch t -tests on Simple Spread ($n = 5$ seeds per condition). Here t is the Welch test statistic, df the Welch-Satterthwaite degrees of freedom, p the two-sided p -value, and Δ the difference in mean success rate in percentage points (pp). The Welch test is used because the collapsed Dynamic LLM variance is incommensurable with the stabilised methods’.

Comparison	t	df	p	Δ (pp)	Verdict
EMA vs Baseline	4.56	5.9	0.006	+12.3	Significant ($p < 0.01$)
Freeze-Schedule vs Baseline	3.06	7.8	0.018	+9.7	Significant ($p < 0.05$)
EMA vs Freeze-Schedule	1.09	6.5	0.32	+2.6	Not significant
Dynamic LLM vs Baseline	-21.4	6.3	< 0.001	-59.2	Highly significant (collapse)

Table A.10: Per-seed results (%) for all environments and methods (seeds 42/101/123/456/999). SR for Spread/LBF, WR for SMAC.

Env	Method	s42	s101	s123	s456	s999	Mean \pm std
Spread	Baseline	76.0	80.1	67.0	70.9	78.2	74.4 \pm 5.4
	EMA $\alpha = 0.2$	87.0	84.9	84.0	86.7	91.0	86.7 \pm 2.7
	Freeze	88.5	88.2	79.7	85.3	78.9	84.1 \pm 4.6
	Dynamic LLM	18.0	11.7	17.6	12.3	16.6	15.2 \pm 3.0
LBF	Baseline	0.0	0.5	0.0	0.1	0.0	0.1 \pm 0.2
	EMA $\alpha = 0.2$	96.5	96.0	92.9	97.0	97.0	95.9 \pm 1.7
	Freeze	93.5	96.0	94.0	92.7	96.0	94.4 \pm 1.5
	Dynamic LLM	95.5	96.0	93.0	92.0	97.0	95.0 \pm 2.4
SMAC	Baseline	99.0	98.7	98.0	99.0	99.2	98.8 \pm 0.5
	EMA $\alpha = 0.2$	100.0	100.0	99.7	100.0	100.0	99.9 \pm 0.1
	Freeze	99.8	100.0	100.0	99.0	100.0	99.8 \pm 0.4
	Dynamic LLM	90.0	98.0	100.0	94.0	100.0	96.4 \pm 4.3

Table A.11: Environment placement under the three-regime taxonomy (QMIX, $n = 5$ seeds). “Best” is the strongest stabilised method (EMA in all three).

Environment	Regime	Baseline	Best
LBF	Essential	0.1%	95.9%
Simple Spread	Augmentative	74.4%	86.7%
SMAC 3m	Supplementary	98.8%	99.9%